Theoretical study on the formation of H- and O-atoms, HONO, OH, NO, and NO_2 from the lowest-lying singlet and triplet states in *ortho*-nitrophenol photolysis

L. Vereecken,[a,b,*] H. K. Chakravarty,[a] B. Bohn,[b] J. Lelieveld[a]

[a] Atmospheric chemistry, Max Planck Institute for Chemistry, 55128 Mainz, Germany

[b] Institute for tropospheric chemistry, Forschungszentrum Jülich GmbH, 52428 Jülich, Germany

[*] corresponding author: L.Vereecken@fz-juelich.de

Abstract

The photolysis of nitrophenols was proposed as a source of reactive radicals and NOx compounds in polluted air. The S_0 singlet ground state and T_1 first excited triplet state of nitrophenol were investigated to assess the energy-dependence of the photofragmentation product distribution as a function of the reaction conditions, based on quantum chemical calculations at the G3SX//M06-2X/aug-cc-pVTZ level of theory combined with RRKM master equation calculations. On both potential energy surfaces we find rapid isomerisation with the *aci*-nitrophenol isomer, as well as pathways forming NO, NO_2, OH, HONO, and H- and O-atoms, extending earlier studies on the T_1 state and in agreement with available work on other nitro-aromatics. We find that accessing the lowest photofragmentation channel from the S_0 ground state requires only 268 kJ/mol of activation energy, but at a pressure of 1 atm collisional energy loss dominates such that significant fragmentation only occurs at internal energies exceeding 550 kJ/mol, making this surface unimportant for atmospheric photolysis. Intersystem crossing to the T_1 triplet state leads more readily to fragmentation, with dissociation occurring at energies of ~450 kJ/mol

above the singlet ground state even at 1 atm. The main product is found to be OH + nitrosophenoxy, followed by formation of hydroxyphenoxy + NO and phenyloxyl + HONO. The predictions are compared against available experimental data.

Table of content graphic

The dominant products from 2-nitro-phenol photolysis are OH, NO, and HONO, which are formed predominantly from the lowest accessible triplet state.

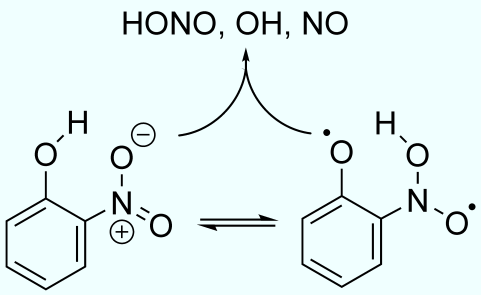

Introduction

Since the first observation of HONO formation from *ortho*-nitrophenol by Bejan et al.[1] a decade ago, the photolysis of *ortho*-nitrophenol is known to be a source of OH radicals[2,3] and HONO.[1] This process was thought to contribute to the concentrations of HONO observed in the troposphere, which were well beyond what was supported by the known HONO sources as implemented in atmospheric models.[4,5] Nitrophenols and other nitrated aromatics are released in the environment from a number of sources, including direct emissions from combustion processes, and *in-situ* formation through the reaction of aromatic radicals with NO_2.[6] The direct OH formation in nitrophenol photolysis, and its indirect formation through HONO photolysis, influences the HOx budget, and hence the oxidative capacity of the atmosphere. Furthermore, nitro-aromatics concentrations are correlated to the NOx levels, and in polluted areas these molecules can be among the pollutants with the highest concentrations, with possible deleterious effects on the biosphere. Their potential impact on health and on the level of reactive radicals in the atmosphere warrants more detailed research into their chemistry. While the observed atmospheric concentrations of *ortho*-nitrophenol do not appear to be high enough to explain the observed tropospheric HONO,[4,6] there remains interest in understanding the photochemical pathways that lead to the formation of HONO, and the competing product channels to other reactive radicals.

The spectroscopic characteristics of nitrophenols have been studied experimentally,[1–3,7–13] revealing large UV absorption cross sections, ~10^{-17} cm^2 $molecule^{-1}$.[7] The photo-induced fragmentation processes in nitrated aromatics are intimately related to the mobility of the H-atoms and NOx moieties, as is evident from both experimental and theoretical studies.[2,3,8,9,13–20] For nitrophenol, the key to the formation of HONO is the *aci*-nitrophenol intermediate (***aci*-NP**), where the phenolic H-atom has migrated to the nitro-moiety to form a –N(O)OH substituent in up to four possible conformers (see Figure 1).

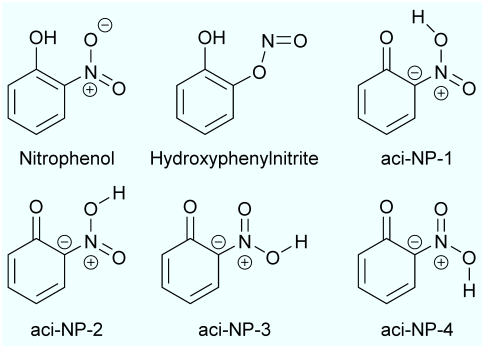

Figure 1: Key intermediates in the photolysis of ortho-nitrophenol. Nitrophenol and aci-nitrophenol exist both as singlet and triplet compounds. Labeling of the aci-nitrophenol compounds follows Wei et al.[2] The depicted Lewis structures show but one of many resonance structures.

The photolysis and subsequent decomposition involves at least the four lowest-lying potential energy surfaces (PES), i.e. the S_0 groundstate and S_1 first excited singlet state, and the two lowest-lying triplet states T_1 and T_2.[3,8,20] Based on experimental data and theoretical work, Ernst et al.[8] conclude that $S_1 \leftarrow S_0$ excitation by a UV photon (see Figure 2) is followed either by subpicosecond relaxation back to the S_0 ground state through a conical intersection, or by an ISC process on a similar time scale to the triplet states.

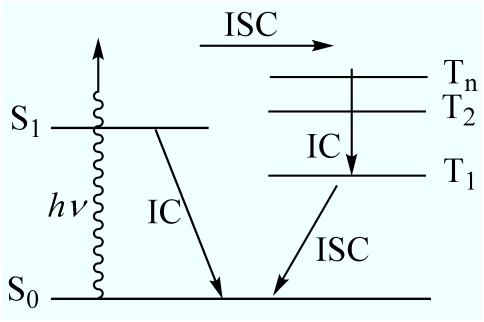

Figure 2: Interstate transitions between several potential energy surfaces in the photolysis of nitrophenol

From these triplet states, they find that HONO can be formed, in competition with vibrational relaxation and ISC back to the S_0 surface. A theoretical MRCI study by Xu et al.[20] identified several additional crossing seams and conical intersections, revealing a complex inter-state photoisomerisation network. Earlier theoretical work on the T_1 triplet surface has characterized exit channels forming HONO or OH.[3] The formation channels for NO and NO_2 were not studied, despite that these reactions are known to play a role in nitro-aromatic photolysis,[15,21] and that these product channels can lead to more energetically favorable products through lower exit energy barriers. The formation of O-atoms and H-atoms is likewise a competitive possibility.[13,22] The S_0 surface has products channels analogous to the T_1 triplet state, within the range of energies afforded by the UV photons employed in the photolysis experiments, but has not been studied in detail before. Photoisomerisation to hydroxyphenylnitrite has been observed experimentally, indicating that the NO_2 moiety is also mobile, with access to both direct and roaming reaction pathways.[21–23]

In this work, we thoroughly investigate the probabilities for O- and H-atom, OH, HONO, NO and NO_2 formation as a function of the internal energy on the two lowest PES S_0 and T_1, by means of quantum chemical and theoretical kinetic studies.

Methodology

a. Quantumchemical calculations

The intermediates and transition states were investigated quantum chemically using M06-2X/aug-cc-pVTZ,[24,25] where zero-point vibrational energy was scaled by 0.971.[26] The relative energies were then refined using the compound G3SX methodology,[27] based on the M06-2X/aug-cc-pVTZ geometries and vibrational characteristics. This level of theory has a mean absolute deviation of ~ 1 kcal mol^{-1} for thermochemistry,[27] though the transition states probably carry a larger uncertainty, estimated to be 2 to 3 kcal mol^{-1}. Broken-symmetry DFT[28] was used for dissociation on the singlet surface forming two radical fragments. Several additional calculations were performed at the M06-2X and B3LYP level of theory, using cc-pVDZ and aug-cc-pVTZ basis sets to asses the stability of the *aci*-nitrophenol conformers (see below); the G3SX//M06-2X/aug-cc-pVTZ level of theory was chosen for the kinetic analysis and is used throughout. The Gaussian-09 software suite[29] was used for all calculations.

b. Theoretical kinetic analysis

RRKM master equation analysis were performed using the DCPD methodology[30] which yields cumulative energy-specific product formation probabilities, i.e. for a given molecule with a certain starting energy content, it traces the probability for irreversibly forming one of the products as determined by the multi-step competition between isomerisation, collisional energy transfer, and dissociation at each intermediate state. Note that this methodology does not assume steady-state conditions. Three models for the reactive system were employed. The first is a rigid-rotor harmonic-oscillator model (RRHO) where all conformers, and their interconvertion, isomerisation and dissociation reactions, are included explicitly. Secondly, we used a lumped, multi-conformer analysis in an RRHO approximation, which assumes that all conformers of a given isomer are in energy-specific statistical equilibrium. Finally, we used a model where the internal rotations are described as simple separable, symmetric one-dimensional hindered torsional degrees of freedom, where the quantum states

are determined as harmonic oscillators below the hindrance potential barrier, and as a free rotor above that barrier.[31,32] Unless stated otherwise, we refer in this work to the product formation probabilities derived using this latter hindered rotor model. Reduced moments of inertia are obtained by the method described by Kilpatrick and Pitzer.[33] Lennard-Jones collision parameters of the $C_6H_5O_3N$ intermediates are estimated as σ = 6.5 Å and ε = 430 K, with an average ΔE_{down} = ~ 300 cm^{-1} in an exponential-down energy transfer model, with air as a bath gas. Thermalization of the intermediates is modeled by collecting in a sink near the bottom of the energy well, such that the cumulative fragmentation yields reported here only include photolytically generated products rather than (slow) thermal decomposition. Barrierless dissociations on the singlet surface are not treated variationally; rather, the rovibrational characteristics used were obtained by constrained optimizations at a single fixed dissociating bond length. According to the variational minimization principle, this approach leads to an overestimation of the contribution of these channels; despite this overestimation, the contribution of these channels remains too small to warrant the computational expense of a (micro-)variational optimization.

Ground state S_0 PES

The kinetically relevant section of the potential energy surface for the S_0 ground state is shown in Figure 3; barrierless fragmentation to OH + nitrophenyl, OH + nitrosooxyphenyl, H + nitrophenoxy, $O(^1D)$ + nitrosophenol, and $O(^1D)$ + oxime (ortho-benzoquinone-mono-oxime) are all highly endothermic by ≥ 410 kJ mol^{-1}, and do not play a significant role. These channels are omitted here but are documented and discussed in the supporting information.

The reactions can be separated into two groups, i.e. the reactions of the singlet nitrophenol (**^{1}NP**) reactant, and of the singlet *aci*-nitrophenol (**^{1}*aci*-NP**) isomers. The isomerisation of **^{1}NP** to **^{1}*aci*-NP** by migration of the phenol H-atom to the NO_2 moiety has a barrier of only 136 kJ mol^{-1}, and can be expected to be rapid at the internal energies afforded by the UV photons. The **^{1}NP** conformers are

planar, with a 36.6 kJ mol^{-1} energy separation between the *cis* and *trans* conformers, as **^{1}*cis*-NP** is stabilized by H-bonding between hydroxy and nitro substituent. Only three of the four possible **^{1}*aci*-NP** isomers depicted in Figure 1 were found to be stable, as **^{1}*aci*-NP-1**, with the H-atom pointing towards the carbonyl oxygen, isomerises without barrier to **^{1}NP**. The **^{1}NP** to **^{1}*aci*-NP** isomerisation transition state is thus a migration with internal rotation in the **^{1}*aci*-NP-2** isomer, in agreement with the findings of Ernst et al.[8]

Internal rotations of the –OH and –N(O)OH moieties then connect the **^{1}*aci*-NP** isomers. In addition, **^{1}*aci*-NP-2** and **^{1}*aci*-NP-3** are connected by an H-migration between the O-atoms in the NO_2 moiety, which has a 36 kJ mol^{-1} lower barrier than –N(O)OH rotation. This is mainly due to the partial double bond character of the C–N bond in **^{1}*aci*-NP** as seen in some of the resonance structures, which hinders rotation of the HONO moiety. Interestingly, the relative barrier heights of this H-shift versus rotation are reversed on the triplet surface (see below).

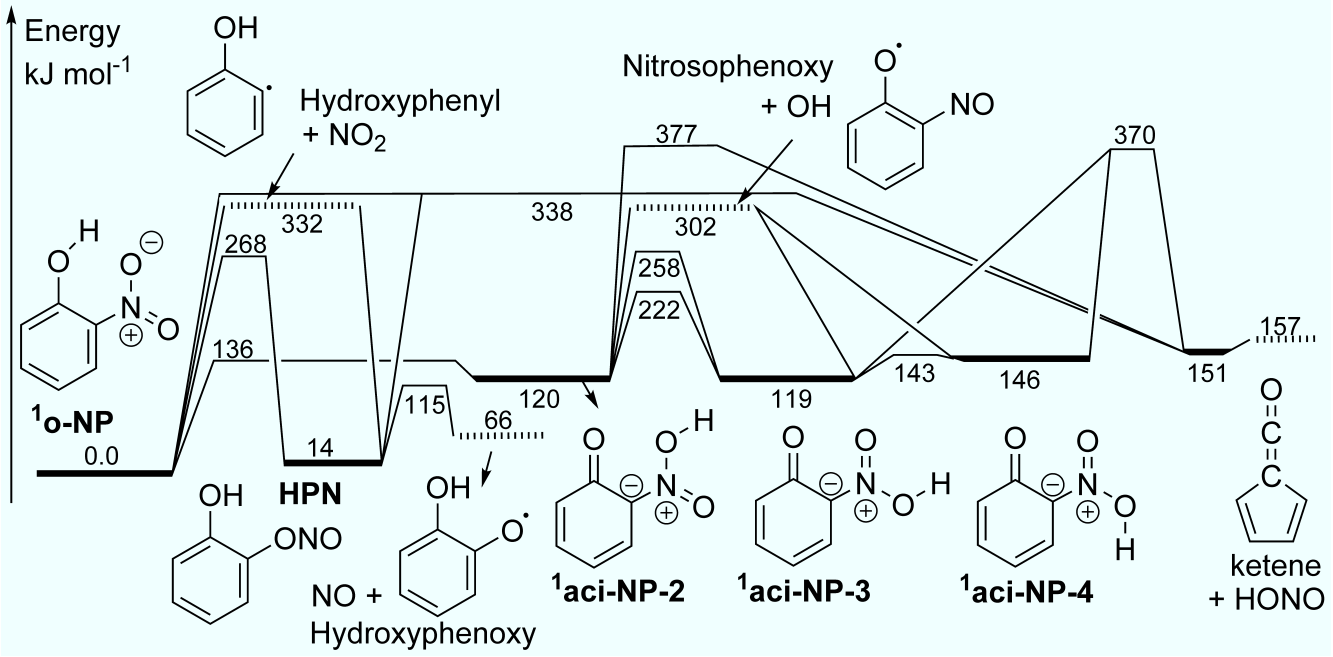

Figure 3: Simplified S_0 singlet potential energy surface at the G3SX//M06-2X/aug-cc-pVTZ level of theory. The depicted Lewis structures each represent only one of many resonance structures. A complete PES and graphical representations of the saddle points are available in the supporting information.

Dissociation of **^{1}NP** can occur through several pathways. Barrierless fragmentation to hydroxyphenyl + NO_2 has an endothermicity of 332 kJ mol^{-1}. Another channel at 268 kJ mol^{-1} involves isomerisation of **^{1}NP** to hydroxyphenylnitrite (**HPN**, 2 stable conformers characterized), through a nitro-nitrite TS as already described for other nitro-aromatics.[15,17,22,23] **HPN** readily fragments to NO + hydroxyphenoxy radicals; this dissociation process is so fast that the **HPN** is not stabilized even in ultra-cold noble gas matrices, when formed from **^{1}NP** isomerisation.[21] Hause et al.[15] showed earlier the existence of a roaming nitro-nitrite isomerisation transition state in nitrobenzene. We were not able to characterize this type of isomerisation for **o-NP**; rather, the roaming of the NO_2 moiety allows abstraction of the phenol H-atom, both in **^{1}NP** and **HPN**, leading to HONO and a cyclic ketene with a five-membered ring. These roaming reactions are the lowest accessible pathways for HONO formation on the singlet surface. Formation of ketenes was described earlier by Cheng et al.[9] for 2-nitrobenzaldehyde, though the current case is fundamentally different as we have a ring size reduction. Finally, **HPN** can also fragment to NO_2 + hydroxyphenyl; this process has a small exit barrier of 7 kJ mol^{-1} above the products at the M06-2X level of theory but this TS becomes submerged by 2 kJ mol^{-1} at the G3SX level of theory, thus suggesting again a barrierless fragmentation as expected for singlet radical-radical interactions.

Two fragmentation channels are shown for **^{1}*aci*-NP**, i.e. barrierless decomposition to OH + nitrosophenoxy, and elimination of HONO forming a ketene with a 5-membered ring (see Figure 3). The formation of HONO shows a distinct energy barrier, despite the stability of the products. These high barriers are again caused by the partial double bond nature of the C=N bond which also hindered the internal HONO rotation. In summary, HONO, NO_2 and NO formation are the energetically lowest-lying dissociation pathways currently characterized from the **^{1}NP** and **HPN** isomers, while OH formation is most favorable from the **^{1}*aci*-NP** isomers.

Due to the reactive attraction between radical fragments on the singlet surface, most of the products do not form stable post-reaction complexes.

First Excited State T_1 PES

Figure 4 shows the kinetically relevant section of the T_1 surface; a more complete PES is depicted in the supporting information and includes the channels forming OH + nitrophenyl, H + nitrophenoxy, and O(^{3}P) + oxime, all of which have barriers to reaction exceeding 430 kJ mol^{-1} relative to the ^{1}**NP** ground state and therefore do not contribute significantly to product formation. As for the ground state, fragmentation on the T_1 surface can be divided into reactions of ^{3}**NP** and of ^{3}***aci*-NP** (see Figure 4). The *cis* and *trans* conformers of ^{3}**NP** are separated only by 10.8 kJ mol^{-1}, and are not planar as the N-atom center has a slight pyramidal geometry of 147°. Contrary to the singlet surface, ^{3}***aci*-NP-1** is more stable than ***cis*-^{3}NP** by 77 kJ mol^{-1}. Only two ^{3}***aci*-NP** isomers were found to exist at the M06-2X/aug-cc-pVTZ level of theory: ^{3}***aci*-NP-1** and ^{3}***aci*-NP-3**. Earlier theoretical work by Cheng et al.[3] using B3LYP/6-311+G(d,p) found three stable conformers (^{3}***aci*-NP-2**, **-3**, and **-4**), and we were indeed able to reproduce these results using B3LYP combined with both the cc-pVDZ and aug-cc-pVTZ basis sets. The M06-2X functional used in this work has a better description of dispersion compared to B3LYP, and is typically better suited to study the relative stability of conformers. Combined with the small cc-pVDZ basis set M06-2X likewise finds the same three *aci*-nitrophenol, but using the larger aug-cc-pVTZ basis set, which better describes longer-range interactions, the ^{3}***aci*-NP-2** isomer becomes unstable towards rotation of the −OH moiety. Extensive efforts to locate an energy minimum for ^{3}***aci*-NP-2** found no stable geometry, despite many variations in starting geometry, DFT integration grids, optimization step sizes, and tracing IRC pathways with small steps for TS that nominally would be expected to yield the ^{3}***aci*-NP-2** isomer. We propose that the earlier ^{3}***aci*-NP-2** geometries[3] were due to the use of small basis sets and DFT functionals with insufficient description of the interaction between

the different moieties, and that this conformer is thus likely only a shoulder on the PES or a vanishingly shallow energy well. At the M06-2X/aug-cc-pVTZ level of theory, the interactions between the acidic H-atom and the radical oxygen atoms in ^{3}***aci*-NP-1** and ^{3}***aci*-NP-3** thus appears to be strong enough to preclude formation of the remaining two isomers. The conformational changes between the ^{3}***aci*-NP** isomers occurs mostly by internal rotation of the –OH and –N(O)OH moieties. As the C–N bond is essentially a single bond on the triplet surface, in contrast to the S_0 singlet surface, internal rotation of –N(O)OH is very facile, with an energy barrier of only a few kJ mol^{-1}. Earlier work by Cheng et al.[3] did not describe this TS, artificially leading to an energy rift separating the ***aci*-NP** isomers in two groups connected only by a higher-energy H-migration between the two oxygen atoms of the NO_2 moiety, for which we find an energy barrier of 115 kJ mol^{-1}. On the triplet surface, ^{3}**NP** has several fragmentation channels available. The highest accessible exit channels shown in Figure 4 are the formation of O(^{3}P) + nitrosophenol, and NO_2 + hydroxyphenyl. The lowest-energy fragmentation pathway, however, is the formation of NO + hydroxyphenoxy, a process that is related to the nitro-nitrite channel on the singlet surface, and was described earlier by Hause et al.[15] for nitrobenzene. At the M06-2X level of theory, this channel involves partial dissociation and rotation of the NO_2 moiety, first forming a spiro-bicyclic structure, which in turn can expel the NO fragment, leaving the hydroxyphenoxy radical as a product.

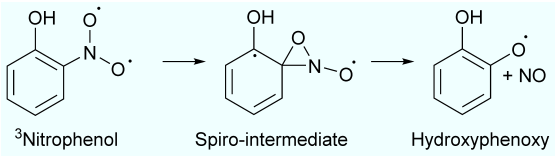

At the G3SX//M06-2X level of theory, however, this second dissociation TS submerges below the spiro intermediate, indicative of a single-step process where the limiting rearrangement is the partial dissociation and rotation of the NO_2 moiety, and in agreement with the pathway found by Hause et al.[15] for nitrobenzene. While the formation of NO + hydroxyphenoxy has a low energy barrier, this transition state is highly rigid and is thus entropically unfavorable.

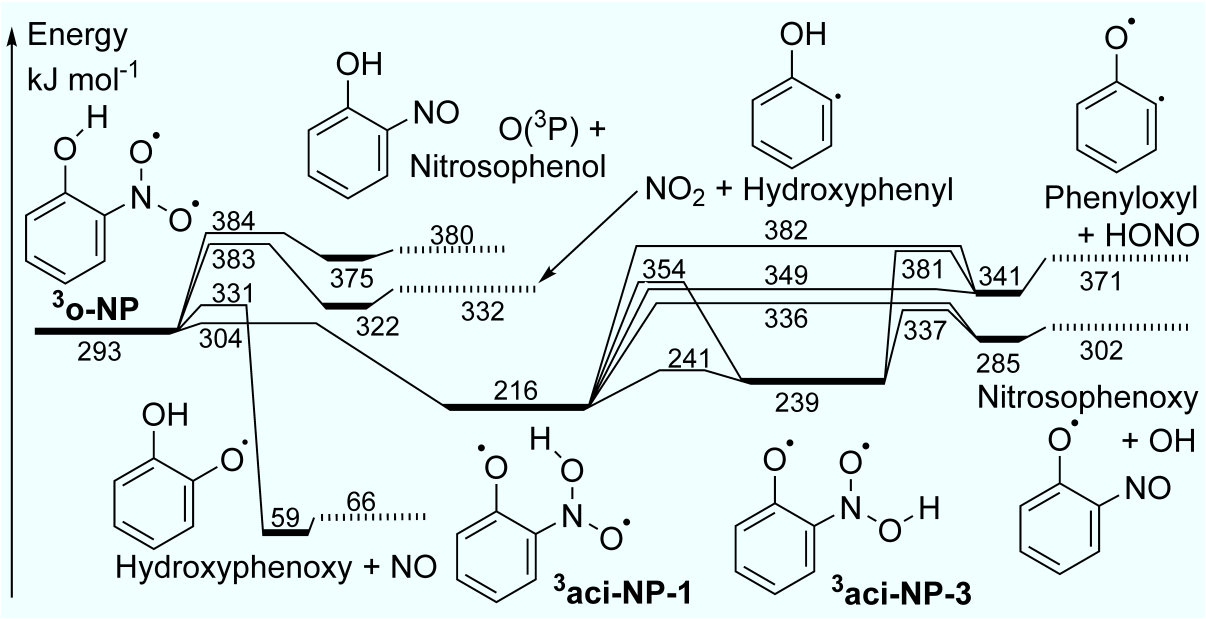

Figure 4: Simplified T_1 triplet potential energy surface at the G3SX//M06-2X/aug-cc-pVTZ level of theory. The depicted Lewis structures each represent only one of many resonance structures. Energies are relative to ^{1}o-NP. A complete PES and graphical representations of the saddle points are available in the supporting information.

The lowest dissociation channel accessible to ^{3}***aci*-NP** isomers was found to be the formation of OH + nitrosophenoxy, while fragmentation to HONO + phenyloxyl has higher exit barriers, in agreement with the relative product stability, and as already described by Cheng et al.[3] The lowest-energy reaction path for *trans*-HONO formation, originating from ^{3}***aci*-NP-1** and with an energy of 349 kJ mol^{-1}, is aided significantly by the formation of a fairly strong product complex with a stability of 30 kJ mol^{-1}. A second pathway forming *cis*-HONO, has a significantly higher barrier at an energy of 382 kJ mol^{-1}; while this TS is geometrically more related to the unstable ^{3}***aci*-NP-2** isomer, IRC calculations connect this pathway to the ^{3}***aci*-NP-1** isomer. ^{3}***aci*-NP-3** likewise leads to the formation of *cis*-HONO. In the atmosphere, *cis*-HONO will readily isomerise to *trans*-HONO, a process that is likely to already occur dynamically during the ^{3}***aci*-NP** dissociation.

Most of the dissociation reactions on the triplet surface lead initially to the formation of post-reaction

complexes, indicated in Figure 4, which are expected to readily fall apart to the separated products.

Energy-specific product formation on S_0

When photochemically excited *ortho*-nitrophenol falls back from either the S_1 or T_1 excited states, it has crossing seams available for both the nitrophenol and the *aci*-nitrophenol isomers. Our master equation analysis show that re-isomerisation between ^{1}**NP** and ^{1}***aci*-NP** is sufficiently fast at all excitation energies studied (up to 800 kJ mol^{-1} above the ^{1}**NP** ground state) for these structures to quickly attain energy-specific steady-state. The product distribution then becomes independent of the isomer initially formed, but rather is a function solely of the nascent internal energy. Figure 5 shows the expected product distribution as a function of the initial internal energy of the ^{1}**NP**/^{1}***aci*-NP** compound at 1 atm and 300 K, where products with negligible yields are omitted. For internal energies below 525 kJ mol^{-1}, the main fate is collisional stabilization as ground state nitrophenol. Stabilization of the higher-energy isomer ^{1}***aci*-NP** has a negligible contribution, as it rapidly isomerises to ^{1}**NP**, and has a low contribution to the steady-state concentration especially at the lower energies. In agreement with the experimental data,[21] we also did not find any stabilization of **HPN**, owing to its rapid decomposition to hydroxyphenoxy + NO. This decomposition TS is sufficiently low in energy that it comprises over 99% of the reaction flux for **HPN** at any energy considered; even re-isomerisation to ^{1}**NP** remains negligible. The ^{1}**NP** kinetics can thus be treated without loss of accuracy by assuming immediate dissociation of the **HPN** isomer to hydroxyphenoxy + NO. Despite that this channel has the lowest exit barrier on the ^{1}**NP** PES, it has only a moderate contribution in the product distribution of up to 10%. The main reason is the rigidity of the nitro-nitrite TS connecting ^{1}**NP** and **HPN**, disfavoring this channel entropically. In fact, as the internal energy increases, the contribution of this channel decreases as higher-lying, but entropically more favorable TS compete more effectively.

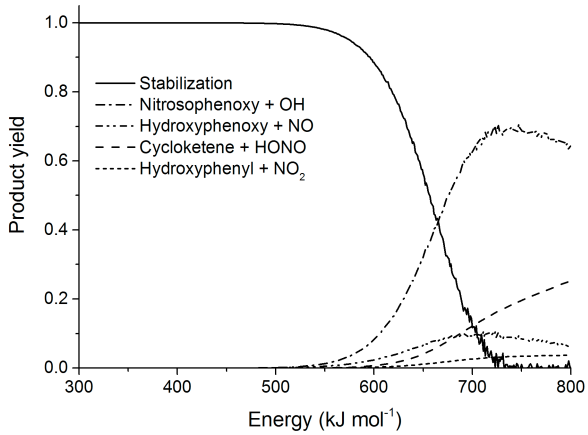

Figure 5: Product distribution at 300 K and 1 atm as a function of the internal energy on the S_0 singlet surface. The noise in the curves is the result of slight numerical instabilities in the calculations.

The main fragmentation product on the S_0 PES is nitrosophenoxy + OH, as expected given that its formation channels are low in energy, and are entropically favorable barrierless dissociations. HONO + cycloketene formation becomes important at higher internal energies. It should be noted that, in contrast to the triplet surface, the main source of HONO is the NO_2 roaming reaction starting from the **^{1}NP** isomer, not the dissociation from **^{1}*aci*-NP**. Full dissociation to hydroxyphenol + NO_2 is predicted to have a somewhat smaller contribution of a few percent. Finally, the high-lying exit channels forming nitrophenyl + OH, nitrosooxyphenyl + OH, nitrophenoxy + H, nitrosophenol + O(^{1}D), and oxime + O(^{1}D) are negligible at all energies considered.

The PES has fragmentation channels that are accessible at the photo-excitation energies used in the experiments, i.e. 243 to 400 nm (490 to 300 kJ mol^{-1}). Our kinetic analysis, however, shows that these internal energies are insufficient to prevent collisional stabilization at 1 atm and fragmentation from the S_0 surface can be neglected. This simplifies further studies of the nitrophenol photolysis system.

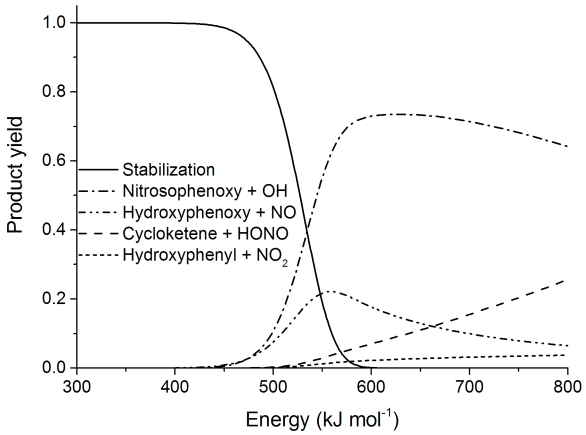

Figure 6: Product distribution at 300 K and 0.01 atm as a function of the internal energy on the S_0 singlet surface.

Reducing the pressure to 0.01 atm (see Figure 6) slows down the collisional energy loss, allowing for a higher contribution of fragmentation at lower internal energies. This mainly benefits dissociation to hydroxyphenoxy + NO through the lowest fragmentation TS. Nitrosophenoxy + OH remains the main product. Even at these lower pressures, however, fragmentation only becomes important at energies above the wavelengths used in the photolysis experiments, and thus above the wavelengths available in the atmosphere. Variations of the temperature has only a very small impact on the product distribution, and is not shown here. The results are somewhat sensitive to the methodology used to describe the kinetics, i.e. an explicit model, a multi-conformer model, or a model using internal rotors. For the main products, this affects the predicted product distributions up to ~ 10% absolute (for most products about a factor of 2 to 3 relative).

Energy-specific product formation on T_1

As the energy wells for the minima on the T_1 triplet energy surface are higher in energy compared to the S_0 surface, while its fragmentation channels have similar energies, dissociation reactions are

significantly faster on the T_1 surface, with an increased contribution of fragmentation as a result.

As shown in Figure 7, fragmentation is active at 1 atm already at 400 kJ mol^{-1} above the **^{1}NP** ground state, in agreement with the experimental data seeing fragmentation products at these energies. Similar to the singlet surface, nitrosophenoxy + OH is the main exit channel. Formation of hydroxyphenoxy + NO through the lowest energy exit channel has a peak contribution at lower energies, but the rigidity of its transition state makes this channel entropically less competitive at higher energies. HONO + phenyloxy formation has a similar contribution as NO formation, growing at higher energies. The formation of hydroxyphenyl + NO_2, and of nitrosophenol + O(^{3}P) remain minor channels that contribute only at high internal energies. The highest exit channels characterized, *i.e.* nitrophenyl + OH, nitrophenoxy + H, and oxime + O(^{3}P), remain negligible at all energies considered.

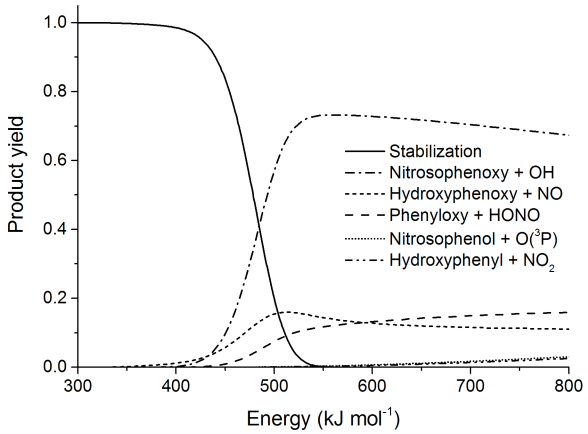

Figure 7: Product distribution at 300 K and 1 atm as a function of the internal energy on the T_1 triplet surface. Energies are relative to the ^{1}o-NP ground state.

At lower pressures, e.g. as shown in Figure 8 for 0.01 atm, collisional stabilization is slower and fragmentation remains possible at even lower energies. Again, we find that this mainly benefits the

lowest-lying, NO-forming channel. The results are not significantly sensitive to the temperature, owing to the large excitation energies and the sharp division between stabilization and fragmentation regimes.

The product distribution does depend slightly on the initial isomer. If ^{3}***aci*-NP** is formed after ISC from S_1 surface, instead of ^{3}**NP**, the fragmentation favors nitrosophenoxy+ OH at high internal energies above 500 kJ mol^{-1}, ultimately adding 10% absolute on the OH yield near 800 kJ mol^{-1} above the ground state (see figure SI-5 and SI-6 in the supporting information). Formation of NO, NO_2, and O(^{3}P) are reduced, while HONO-formation remains at a similar level of up to 20%. This shift is the result of the comparatively low energy difference between isomerisation and dissociation TS, such that isomerisation rate between ^{3}**NP** and ^{3}***aci*-NP** isomers does not overwhelm the dissociation, and the population does not fully reach energy-specific equilibrium across all isomers prior to fragmentation. This prevents simplification of the theoretical treatment of nitrophenol photolysis at high energies. The results are moderately sensitive to the methodology used to describe the kinetics. Specifically, the harmonic oscillator multi-conformer analysis finds lower NO and HONO yield than the fully explicit model or the internal rotor model. All three results, however, remain within ~ 10% absolute, and lead to the same main conclusions.

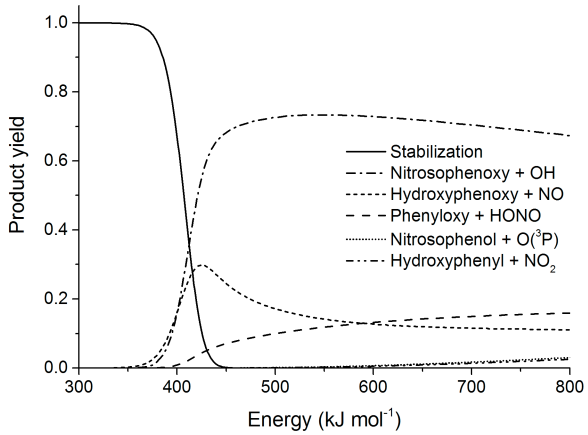

Figure 8: Product distribution at 300 K and 0.01 atm as a function of the internal energy on the T_1 triplet surface. Energies are relative to the ^{1}o-NP ground state.

Comparison to experiment

Cheng et al.[3] conducted experiments at 200 mTorr and 298 K, with photolysis energies ranging from 306 to 332 kJ mol^{-1} (391 to 360 nm) plus ~ 12 kJ mol^{-1} thermal internal energy. OH was observed to be formed cold ($\upsilon = 0$) with a rotational energy of only 8 ± 0.8 kJ mol^{-1}. Earlier work by Wei et al.[2] in the same research group found similar results at 266 and 355 nm. These observations are fully compatible with the OH + nitrosophenoxy energy predicted theoretically at 302 kJ mol^{-1}. Master equation calculations for the low-pressure reaction conditions of these experiments (see supporting information), however, find the onset of significant OH formation on the triplet surface at energies above ~ 370 kJ mol^{-1}, shifted downwards by 25 kJ mol^{-1} from the plot in Figure 8 but still somewhat higher than the lowest average energies available in the experiments. This is due partly to the exit barriers calculated at energies of 336 kJ mol^{-1}, and could indicate that these barriers are slightly overestimated. The predicted appearance energy for OH is further increased by some collisional stabilization at energies just above the dissociation TS, and could indicate that collisional stabilization is overemphasized compared to dissociation in the current Master equation calculations. At the same time, one should consider that the

thermal Boltzmann energy distribution of o-NP is at least 30 kJ mol^{-1} wide (comprising 90% of the population) with an extended tail at higher energies; the energy requirements can thus be met, albeit with a lower yield. Cheng et al. observe a ~30 % increase of OH yield with photon energies increasing from 380 to 360 nm. Assuming an energy distribution for the triplet state equal to a shifted thermal Boltzmann distribution of ^{1}o-NP, and assuming a purely monochromatic excitation light source, our predictions indicate a much steeper increase in OH yield of about an order of magnitude, as in this energy range we find the sudden onset of significant fragmentation to OH. If this onset would be shifted in the theoretical predictions to lower energies, or if the excitation photons would have a non-monochromatic energy distribution, this would strongly dampen the impact of the excitation energy on the yields. On the S_0 singlet surface, even the low pressures used by Cheng et al. do not allow for significant OH formation at energies below 400 kJ mol^{-1}; it is unclear whether the observed OH could originate partly from other excited states for the given energies.

The experiments of Bejan et al.[1] were performed at 1 atm and 298 K, photolysing with a broad spectral peak with a maximum around 370 nm, affording photolysis energies ranging from 239 to 399 kJ mol^{-1} (500 to 300 nm) plus ~ 12 kJ mol^{-1} thermal internal energy. They observed formation of HONO, whose yield changed by up to a factor of 3 when changing the bath gas from N_2 to Ar, O_2, synthetic air, and He. Despite that o-NP is an efficient absorber, the quantum yields observed were very small, ~10^{-4}, which indicates an inefficient fragmentation process at the selected excitation energies. No significant NO_2 formation was observed. Our predictions for the T_1 surface (Figure 7) using air as a bath gas show only small HONO yields at the employed energies, ranging from 0 to 5×10^{-4}. The HONO yield is in the fall-off region of pressures, which agrees with the experimental dependence of the yield on changes to the bath gas. The predicted yield of HONO is fairly sensitive to the collisional energy transfer characteristics used in the master equation calculations, and the onset of the fall-off regime is thus subject to fairly large uncertainties of > 10 kJ mol^{-1}, such that experiment and theory are not in

disagreement within these uncertainties. Importantly, at the energies for this experiment we predict that yields of nitrosophenoxy + OH, and hydroxyphenoxy + NO are significantly higher than HONO formation. HONO formation on the S_0 surface is negligible at the photolysis energies employed.

Recent experiments by Grygoryeva et al.[13] looked at the H-atom fragment kinetic energy distributions for a set of (nitro)phenols irradiated with 243 nm photons. From the comparison between phenol and 2-nitrophenol they conclude that the H-atom in o-NP is mobile, preventing the expulsion of fast H-atoms as happens in phenol. Their maximum measured H-fragment kinetic energy, and their quantum chemical calculations, are in good agreement with our O–H bond dissociation enthalpy of 410 kJ mol^{-1} at the G3SX//M06-2X level of theory. We predict negligible formation yields for H-atoms from both the T_1 and the S_0 state, such that the observed H-fragments are likely formed from another excited state. Indeed, Grygoryeva et al. discuss excitation to several higher excited states; the $n\pi^*$ state specifically is a non-dissociative surface that leads to H-migration between o-NP and aci-NP, and is the cause of the qualitative differences in the H-atom velocities between phenol and o-NP photofragmentation. These higher excited states are outside the scope of the current work.

Conclusions

In this work, we have characterized the S_0 and T_1 potential energy surfaces for nitrophenol using the G3SX//M06-2X/aug-cc-pVTZ level of theory. Several new fragmentation and isomerisation channels were found, allowing access to formation of HONO, NO, NO_2, OH, and H- and O-atoms from both PES. This work thus extends earlier work that focused only on the channels leading to OH and HONO, and brings it in line with theoretical and experimental work on other nitroaromatics.

A kinetic analysis gave semi-quantitative insights in the behavior of this system. The results presented here are not sufficient to obtain fragmentation quantum yields for nitrophenol photolysis, as they need

to be embedded in a more complete scheme that quantifies the surface hopping dynamics between the lowest-lying singlet and triplet states, containing at least the S_0, S_1, T_1 and T_2 states. Fragmentation from higher-lying states such as the S_1 and T_2 states has not been considered here, though these states are known to play a role in *ortho*-nitrophenol photolysis. The characterization of these states, and the quantification of the IC and ISC rates are outside the scope of the present work.

For the S_0 ground state, we conclude that the photolysis wavelengths used in the experiments, or those available in the atmosphere, do not afford sufficient internal energy to allow significant fragmentation at ambient conditions, and collisional stabilization of the excited nitrophenol or *aci*-nitrophenol compounds back to thermalized nitrophenol is the primary fate even at pressures as low as 0.01 atm This conclusion is robust against variations of the kinetic model.

For the T_1 state, we find that formation of OH, HONO, and NO are the main fragmentation channels, while NO_2, H, and O(^{3}P) yields remain low. HONO, OH and NO are thus expected to be formed upon nitrophenol photolysis in the atmosphere. The predicted yields depend for up to ~10% absolute on the kinetic model used, e.g. explicit versus lumped conformer models, and harmonic oscillator versus internal rotor methodologies, such that a sufficiently rigorous theoretical kinetic framework is recommended for future quantitative work. We also find that the product distribution at very high energies appears to be somewhat sensitive to the isomeric form after ISC from the S_1 state, i.e. if the ISC processes follows a crossing seam forming ^{3}**NP** versus ^{3}***aci*-NP**, a slightly different product distribution is expected, where nascent formation of the latter isomer increases OH and HONO formation to some extent, to the detriment of NO formation. This effect should not play at typical solar photo-energies.

A comparison with available product measurements seems to suggest that the theoretically predicted product formation occurs at a slightly higher internal energy than indicated by the experimental data, though this comparison is tentative only. An overestimation of the collisional stabilization rate would

be the most likely cause of this discrepancy, but as experimental product yields of sufficient quality are currently not available, we did not attempt to calibrate the collision model.

While there is qualitative agreement between the theoretical results and the experimental observations, it is clear that more work is needed. Firstly, there are product channels predicted by theory that have not been observed as yet, where NO formation in particular could be of importance. Secondly, compared to experiment, the current kinetic calculations might be overestimating collisional stabilization. The theoretical work does show that the reaction is expected to be rather sensitive to the reaction conditions, such as pressure and spectral characteristics, as the induced fragmentation is in the fall-off regime at the relevant energies. In this respect, it would be useful to have experiments that more faithfully reflect ambient conditions, i.e. 1 atm of air, and a spectral source that includes the solar UV-B (~300 nm) and higher-energy radiation. The theoretical analysis needs to be augmented with a quantification of the inter-surface hopping kinetics to derive an overall quantum yield for fragmentation.

Acknowledgments

H.K.C. was supported under project VE 731/1-1 of the Deutsche Forschungsgemeinschaft (DFG), Germany. L.V. gratefully recognizes the support of the Max Planck Graduate Center with the Johannes Gutenberg-Universität Mainz (MPGC), Germany, for part of this research.

Supporting information

Extended S_0 and T_1 PES; figures for TS geometries; figures for product yields; geometries, rovibrational characteristics and energies of structures discussed in the text, at various levels of quantum chemical theory.

Bibliography

(1) Bejan, I.; Abd El Aal, Y.; Barnes, I.; Benter, T.; Bohn, B.; Wiesen, P.; Kleffmann, J. Phys Chem Chem Phys 2006, 8 (17), 2028–2035.
(2) Wei, Q.; Yin, H.-M.; Sun, J.-L.; Yue, X.-F.; Han, K.-L. Chem Phys Lett 2008, 463 (4–6), 340–344.
(3) Cheng, S.-B.; Zhou, C.-H.; Yin, H.-M.; Sun, J.-L.; Han, K.-L. J Chem Phys 2009, 130 (23), 234311.
(4) Li, X.; Rohrer, F.; Hofzumahaus, A.; Brauers, T.; Haeseler, R.; Bohn, B.; Broch, S.; Fuchs, H.; Gomm, S.; Holland, F.; Jaeger, J.; Kaiser, J.; Keutsch, F. N.; Lohse, I.; Lu, K.; Tillmann, R.; Wegener, R.; Wolfe, G. M.; Mentel, T. F.; Kiendler-Scharr, A.; Wahner, A. Science 2014, 344 (6181), 292–296.
(5) Spataro, F.; Ianniello, A. J Air Waste Manag Assoc 2014, 64 (11), 1232–1250.
(6) Harrison, M. a. J.; Barra, S.; Borghesi, D.; Vione, D.; Arsene, C.; Olariu, R. L. Atmos Environ 2005, 39 (2), 231–248.
(7) Chen, J.; Wenger, J. C.; Venables, D. S. J Phys Chem A 2011, 115 (44), 12235–12242.
(8) Ernst, H.; Wolf, T. J. A.; Schalk, O.; González-García, N.; Boguslavskiy, A. E.; Stolow, A.; Olzmann, M.; Unterreiner, A.-N. J Phys Chem A 2015, 119 (35), 9225–9235.
(9) Cheng, S.-B.; Zhou, C.-H.; Yin, H.-M.; Sun, J.-L.; Han, K.-L. Chemphyschem 2009, 10 (7), 1135–1142.
(10) Kovacs, A.; Izvekov, V.; Keresztury, G.; Pongor, G. Chem Phys 1998, 238 (2), 231–243.
(11) Nagaya, M.; Kudoh, S.; Nakata, M. Chem Phys Lett 2006, 427 (1–3), 67–71.
(12) Wang, Y.-Q.; Wang, H.-G.; Zhang, S.-Q.; Pei, K.-M.; Zheng, X.; Lee Phillips, D. J Chem Phys 2006, 125 (21), 214506.
(13) Grygoryeva, K.; Kubečka, J.; Pysanenko, A.; Lengyel, J.; Slavíček, P.; Fárník, M. J Phys Chem A 2016, DOI: 10.1021/acs.jpca.6b04459.
(14) Borisenko, K. B.; Bock, C. W.; Hargittai, I. J Phys Chem 1994, 98 (5), 1442–1448.
(15) Hause, M. L.; Herath, N.; Zhu, R.; Lin, M. C.; Suits, A. G. Nat Chem 2011, 3 (12), 932–937.
(16) Heintz, A.; Kapteina, S.; Verevkin, S. P. J Phys Chem A 2007, 111 (28), 6552–6562.
(17) Polášek, M.; Tureček, F.; Gerbaux, P.; Flammang, R. J Phys Chem A 2001, 105 (6), 995–1010.
(18) Shenghur, A.; Weber, K. H.; Nguyen, N. D.; Sontising, W.; Tao, F.-M. J Phys Chem A 2014, 118 (46), 11002–11014.
(19) Simperler, A.; Lampert, H.; Mikenda, W. J Mol Struct 1998, 448 (2–3), 191–199.
(20) Xu, C.; Yu, L.; Zhu, C.; Yu, J. J Phys Chem A 2015, 119 (42), 10441–10450.
(21) Nagaya, M.; Kudoh, S.; Nakata, M. Chem Phys Lett 2006, 432 (4–6), 446–451.
(22) Yang, R. J.; Jin, X.; Wang, W. N.; Fan, K. N.; Zhou, M. F. J Phys Chem A 2005, 109 (19), 4261–4266.
(23) Yu, T.; Mebel, A. M.; Lin, M. C. J Phys Org Chem 1995, 8 (1), 47–53.
(24) Zhao, Y.; Truhlar, D. G. Theor Chem Acc 2008, 120 (1–3), 215–241.
(25) Dunning, T. H. J Chem Phys 1989, 90 (2), 1007–1023.
(26) Alecu, I. M.; Zheng, J.; Zhao, Y.; Truhlar, D. G. J Chem Theory Comput 2010, 6 (9), 2872–2887.
(27) Curtiss, L. A.; Redfern, P. C.; Raghavachari, K.; Pople, J. A. J Chem Phys 2001, 114, 108–117.
(28) Noodleman, L. J Chem Phys 1981, 74 (10), 5737–5743.
(29) Frisch, M. J.; Trucks, G. W.; Schlegel, H. B.; Scuseria, G. E.; Robb, M. A.; Cheeseman, J. R.; Scalmani, G.; Barone, V.; Mennucci, B.; Petersson, G. A.; Nakatsuji, H.; Caricato, M.; Li, X.; Hratchian, H. P.; Izmaylov, A. F.; Bloino, J.; Zheng, G.; Sonnenberg, J. L.; Hada, M.; Ehara, M.;

Toyota, K.; Fukuda, R.; Hasegawa, J.; Ishida, M.; Nakajima, T.; Honda, Y.; Kitao, O.; Nakai, H.; Vreven, T.; Montgomery Jr., J. A.; Peralta, J. E.; Ogliaro, F.; Bearpark, M.; Heyd, J. J.; Brothers, E.; Kudin, K. N.; Staroverov, V. N.; Keith, T.; Kobayashi, R.; Normand, J.; Normand, J.; Raghavachari, K.; Rendell, A.; Burant, J. C.; Iyengar, S. S.; Tomasi, J.; Cossi, M.; Rega, N.; Millam, J. M.; Klene, M.; Knox, J. E.; Cross, J. B.; Bakken, V.; Adamo, C.; Jaramillo, J.; Gomperts, R.; Stratmann, R. E.; Yazyev, O.; Austin, A. J.; Cammi, R.; Pomelli, C.; Ochterski, J. W.; Martin, R. L.; Morokuma, K.; Zakrzewski, V. G.; Voth, G. A.; Salvador, P.; Dannenberg, J. J.; Dapprich, S.; Daniels, A. D.; Farkas, O.; Foresman, J. B.; Ortiz, J. V.; Cioslowski, J.; Fox, D. J.; Pople, J. A. *Gaussian 09, Revision B.01*; Gaussian Inc.: Wallington CT, 2010.

(30) Vereecken, L.; Huyberechts, G.; Peeters, J. J Chem Phys 1997, 106 (16), 6564–6573.

(31) Barker, J. R.; Shovlin, C. N. Chem Phys Lett 2004, 383 (1–2), 203–207.

(32) Troe, J. J Chem Phys 1977, 66 (11), 4758–4775.

(33) Kilpatrick, J. E.; Pitzer, K. S. J Chem Phys 1949, 17 (11), 1064–1075.